UNIVERSITY OF AMSTERDAM

UvA-DARE (Digital Academic Repository)

The spectroscopy of high Rydberg states of ammonia

Morgan, R.A.; Langford, S.R.; Orr-Ewing, A.J.; Western, C.M.; Ashfold, M.N.R.; Buma, W.J.; Rijkenberg, A.; de Lange, C.A.; Scheper, C.R.

Link to publication

The spectroscopy of high Rydberg states of ammonia

Stephen R. Langford, Andrew J. Orr-Ewing, Ross A. Morgan, Colin M. Western,
and Michael N. R. Ashfold
School of Chemistry, University of Bristol, Cantock's Close, Bristol BS8 1TS, United Kingdom

Arjan Rijkenberg, Connie R. Scheper, Wybren Jan Buma, and Cornelis A. de Lange
*Laboratory for Physical Chemistry, University of Amsterdam, Nieuwe Achtergracht 127,
1018 WS Amsterdam, The Netherlands*

This paper extends our knowledge of the higher excited states of the ammonia molecule by presenting detailed measurements of the $2+1$ resonance enhanced multiphoton ionization (REMPI) spectrum of both NH_3 and ND_3 obtained following excitation in the wavelength range 298–242 nm, i.e., at energies up to the first ionization energy. Complementary analyses of the wavelength resolved REMPI spectrum and the accompanying REMPI-photoelectron spectra leads to the identification of ten new Rydberg origins of NH_3 (four for ND_3) with principal quantum numbers $n \leq 8$ and, in most cases, of the accompanying out-of-plane bending vibrational progression. Symmetry assignments for the various newly identified excited states are offered, based on band contour simulation and/or quantum defect considerations. Dominant amongst these are the $\widetilde{E}'' \ ^1A_2''$ ($5sa_1' \leftarrow 1a_2''$) state: $\nu_0 = 74\,118(2)$ cm^{-1} [NH_3], $\nu_0 = 74\,258(2)$ cm^{-1} [ND_3], the $\widetilde{F}'' \ ^1E''$ ($5pe'$ $\leftarrow 1a_2''$) state: $\nu_0 = 76\,220(50)$ cm^{-1} [NH_3], $\nu_0 = 76\,240(50)$ cm^{-1} [ND_3], the $\widetilde{F}' \ ^1A_1'$ ($5pa_2''$ $\leftarrow 1a_2''$) state: $\nu_0 = 76\,674(1)$ cm^{-1} [NH_3], $\nu_0 = 76\,770(5)$ cm^{-1} [ND_3], and the $\widetilde{G}' \ ^1A_1'$ ($6pa_2''$ $\leftarrow 1a_2''$) state: $\nu_0 = 78\,494(1)$ cm^{-1} [NH_3]. The present work serves to reinforce the previously noted dominance of $np \leftarrow 1a_2''$ Rydberg excitations in the $2+1$ REMPI spectrum of ammonia. In addition, the adiabatic ionization energy of ND_3 is estimated to be $82\,280 \pm 40$ cm^{-1} based on the assumption that analogous Rydberg states of NH_3 and ND_3 will have very similar quantum defects. © *1998 American Institute of Physics.* [S0021-9606(98)00516-9]

I. INTRODUCTION

The excited electronic states of ammonia have attracted much experimental and theoretical attention over the years, focusing on their spectroscopy, their complex predissociation pathways, and, in some cases, their detailed photochemistry. Much of the early spectroscopic work used conventional ultraviolet (uv) and, particularly, vacuum ultraviolet (vuv) gas phase absorption to elucidate the vertical electronic spectrum.[1–5] The detailed current level of understanding owes much to the introduction of multiphoton excitation spectroscopies allied with jet-cooling techniques and the publication of the seminal papers of Colson and co-workers in the late 1970s.[6,7] The reason for this is one of spectral congestion. All the observed excited electronic states of ammonia below the first ionization energy (IE) are formed by the promotion of an electron from the doubly occupied $3a_1$ nitrogen lone pair orbital in the pyramidal (C_{3v}) ground state to Rydberg orbitals with principal quantum number $n \geq 3$, resulting in states with planar (D_{3h}) equilibrium geometries. As a result, each electronic transition appears with a long vibrational progression associated with excitation of the out-of-plane mode ν_2'. This density of vibronic structure, compounded by the spectral line broadening due to predissociation of many of these excited states, proved a major encumbrance to definitive assignment. Multiphoton absorption methods, and in particular the technique of resonance enhanced multiphoton ionization (REMPI), offer comple-

mentary selection rules and, more importantly, reveal just the less predissociated (i.e., more long lived) excited electronic states.[8] These benefits, when coupled with jet-cooling of the target molecule, have led to major advances in our description of the excited electronic states of ammonia.

Colson's group[6,7] recorded and compared the three-photon REMPI spectra and the one-photon vuv absorption spectra of both NH_3 and ND_3 over the wavenumber range ca. $62\,500–80\,000$ cm^{-1} and provided what is, to date, the most complete global description of the electronic spectrum of ammonia. Much of the subsequent work has been concerned with extending and refining parts of this spectroscopic analysis and/or with detailed analysis of the predissociation mechanisms affecting some of the lower lying Rydberg states.

The small size and high symmetry of ammonia encourages description of its molecular orbitals within the united atom approximation,[3,9,10] in this case a neon atom. Figure 1 shows the observed electronic origin energies of some of the possible excited states of NH_3, labeling the Rydberg orbitals in terms of a neon atom split in a field of D_{3h} symmetry. This is appropriate for the case of the planar Rydberg states studied here and explains our use of the $1a_2''$ symmetry label for the HOMO (rather than the $3a_1$ label applicable if ammonia were a rigid C_{3v} molecule). Only states with principal quantum number $n \leq 5$ are shown in the figure; higher states will derive from the same orbital pattern and the figure
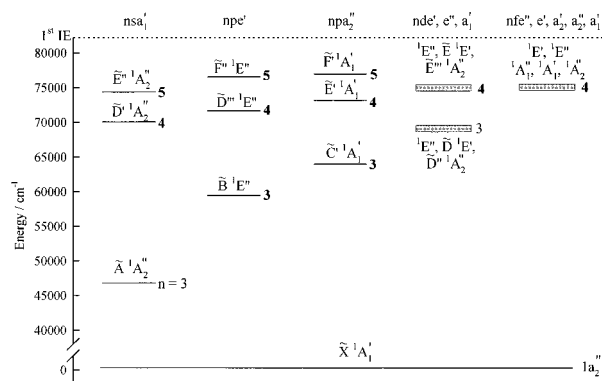
FIG. 1. Orbital correlation diagram for NH_3 up to the principal quantum number $n = 5$, plotting the term values (ν_0) of the observed excited Rydberg states belonging to the five series discussed in this study. The label (following Ref. 7) and symmetry of each state is also given, along with the corresponding value of the principal quantum number n. The type of Rydberg electron orbital associated with each series, cast in terms of a united atom (Ne) in a D_{3h} field, is supplied at the top of each "column" of states. The values of n which are printed in bold indicate that the associated states have been observed in a MPI study.

should therefore help the reader when states with higher n are discussed later in the text.

The $\widetilde{A}\ {}^1A_2'' \leftarrow \widetilde{X}\ {}^1A_1'$ absorption spectrum of NH_3 shows vibronic structure but no rotational fine structure and only the 0_0^0 and 2_0^1 bands of the $ND_3(\widetilde{A}\text{-}\widetilde{X})$ system show resolvable rotational structure.[3] The recent understanding of this efficient (picosecond time scale) predissociation has come in part from rotational lifetimes and decay rates deduced from simulation of individual $\widetilde{A}\leftarrow\widetilde{X}$ vibrational band contours[11] and from direct linewidth measurements of fully resolved rovibrational transitions observed via double resonance methods, e.g., by stimulated emission pumping (SEP) following multiphoton preparation of $\widetilde{C}'$ state molecules[12,13] or in microwave-optical double resonance experiments.[14] Coupled with *ab initio* calculations of the $\widetilde{A}$ state potential-energy surface,[15] measurements and modeling of the energy disposal,[16,17] and the recoil velocity and angular momentum vector correlations[18,19] in the NH_2 photofragments, these studies have afforded a remarkably detailed picture of the photofragmentation dynamics of $\widetilde{A}$ state ammonia molecules.

The electronic promotion $3pe' \leftarrow 1a_2''$ gives rise to the $\widetilde{B}\ {}^1E'' \leftarrow \widetilde{X}\ {}^1A_1'$ system of ammonia. The associated 2_0^n vibronic progressions in both NH_3 and ND_3 have been identified in one-photon vuv absorption.[1–3,20,21] Our knowledge of the $\widetilde{B}$ state has been greatly enhanced by two-photon REMPI spectroscopy studies both under beam conditions[22] and, with sub-Doppler resolution, in the bulk.[23] The latter study yielded molecule limited linewidths of individual $ND_3(\widetilde{B}\text{-}\widetilde{X})$ rovibronic transitions, thereby enabling determination of a (rotational level independent) lifetime of ~0.25 ns for levels of the $ND_3(\widetilde{B})$ state with $\nu_2' \lesssim 6$. Our knowledge of the predissociation dynamics of vibrational levels of the $\widetilde{B}$ state in NH_3 and ND_3 has been extended subsequently by $(2+1')$ two-color pump–probe ionization on a picosecond time scale in combination with high-resolution photoelectron

spectroscopy.[24] Clarification of the extent of Jahn–Teller distortion affecting the degenerate $\widetilde{B}$ state has come from a number of rotationally resolved double resonance studies in which $\widetilde{B}$ state levels associated with excitation of one quantum of each of the doubly degenerate vibrations ν_3' and ν_4',[25] built on a progression in ν_2', were populated following initial excitation of molecules into selected rovibrational levels of the $\widetilde{X}$[26–28] or $\widetilde{A}$[29,30] states. These studies also showed that the historically labeled $\widetilde{C}\text{-}\widetilde{X}$ system of ammonia actually involves a vibronic component of the $\widetilde{B}$ state.

The $\widetilde{C}' \leftarrow \widetilde{X}\ 2_0^n$ progressions in NH_3 and ND_3 were first revealed in the multiphoton study of Nieman and Colson who established the ${}^1A_1'$ electronic symmetry of the $\widetilde{C}'$ state.[6] The spectroscopy and predissociation of these $\widetilde{C}'(\nu_2')$ levels have since been investigated further using both $3+1$ (Ref. 31) and sub-Doppler $2+1$[32] REMPI techniques as well as real-time pump–probe REMPI-PES studies on a ps time scale.[24] Analysis of the widths and intensities of individual rovibrational features in the $\widetilde{C}'\text{-}\widetilde{X}$ multiphoton excitation spectrum provided evidence for two competing predissociation mechanisms: a homogeneous predissociation (i.e., involving coupling to one or more states of the same vibronic symmetry, the efficiency of which is thus independent of parent rotation) presumably involving the $\widetilde{A}\ {}^1A_2''$ state, and a heterogeneous route promoted by in-plane $(x,y$ axis) rotation which was attributed to Coriolis induced predissociation via the $\widetilde{B}\ {}^1E''$ state. These data, quantum defect considerations, and the results of companion REMPI-PES experiments[33–35] which show a strong propensity for the final one-photon ionization step to be Franck–Condon diagonal in all vibrational modes, all indicate that the $\widetilde{C}'\ {}^1A_1'$ state is the first $(n=3)$ member of the $npa_2'' \leftarrow 1a_2''$ Rydberg series of ammonia. Double resonant multiphoton excitation (via the $\widetilde{A}$ state) to this electronic state has also allowed an unambiguous identification of the ν_1 symmetric stretching mode in the $\widetilde{C}'$ state of both NH_3 and ND_3.[29] The former was also identified in an earlier careful REMPI-photoelectron spectroscopy (PES) study of jet-cooled NH_3.[36]

Recent experiments by Li and Vidal[21] have investigated features associated with the $\widetilde{D} \leftarrow \widetilde{X}\ 2_0^n$ progression in the one-photon vuv excitation spectrum of both NH_3 and ND_3, by monitoring either fluorescence from the fraction of $NH_2(ND_2)$ photofragments that are formed in their excited $\widetilde{A}\ {}^2A_1$ state or parent ions that result from absorption of a visible photon by the vuv prepared state (i.e., $1+1'$ REMPI). The features observed in the NH_3 spectrum were too broad to allow determination of any upper state rotational constants or to verify the previously proposed[7] ${}^1E''$ excited state symmetry. However, a band contour simulation of the less predissociation broadened $\widetilde{D}\text{-}\widetilde{X}\ 0_0^0$ transition in ND_3, recorded under both beam and bulk conditions, shows conclusively that the $\widetilde{D}$ state in fact has ${}^1E'$ symmetry, consistent with it being derived from the electronic promotion $3de'' \leftarrow 1a_2''$.[21] The $\widetilde{D}'\ {}^1A_2'' \leftarrow \widetilde{X}$, $\widetilde{D}''\ {}^1A_2'' \leftarrow \widetilde{X}$, and $\widetilde{D}'''\ {}^1E'' \leftarrow \widetilde{X}$ transitions (attributable to the respective orbital promotions $4sa_1' \leftarrow 1a_2''$, $3da_1' \leftarrow 1a_2''$, and $4pe' \leftarrow 1a_2''$) lie in the same energy region (Fig. 1) and have been identified via vuv ab-

sorption and/or $3+1$ REMPI spectroscopy.[7] Symmetry considerations dictate that the $^1E''(3de'\leftarrow 1a_2'')$ excited state must lie in this energy range also but this state has yet to be identified.

The highest energy Rydberg state of ammonia reported hitherto at a level of rotational resolution is the $\widetilde{E}'\ ^1A_1'(4pa_2''\leftarrow 1a_2'')$ state. A recent $2+1$ REMPI study and accompanying band contour simulations[37] yielded excited-state spectroscopic parameters for both NH_3 and ND_3 and some insight into the predissociation behavior of the observed 2^n levels, all of which show many parallels with existing knowledge of the corresponding $\widetilde{C}'\ ^1A_1'(3pa_2''\leftarrow 1a_2'')$ excited state.

At yet higher energies, but still below the first IE ($E_i=82\,159\ \mathrm{cm}^{-1}$ in the case of NH_3[38]), the $\widetilde{F}\ ^1A_2''$ and $\widetilde{G}\ ^1A_2''$ Rydberg states have been identified via their respective 2_0^n progressions in the vuv absorption spectrum[1,4,39,40] and assigned in terms of the electron promotion $nsa_1'\leftarrow 1a_2''$, $n=6$ and 7, respectively. However, even the more recent experiments involving jet-cooled samples[39,40] had insufficient resolution to permit any rotational analysis of these features.

The present study is intended to complement and extend all previous MPI and vuv absorption studies of ammonia and provide a comprehensive picture of the two-photon resonant MPI spectrum of jet-cooled NH_3 and ND_3 molecules at energies above the $\widetilde{C}'$ state origin and up to the first ionization limit. A parallel study measuring the kinetic energies of the photoelectrons that accompany the various MPI resonances proved to be of decisive importance in obtaining the proper assignment of these resonances and have in fact allowed us to determine unambiguously their vibrational quantum numbering. We identify ten new electronic origins for NH_3 (four in the case of ND_3), out-of-plane bending progressions associated with the majority of them, and offer a coherent assignment of the various electronic states based on band contour simulations and/or quantum defect considerations.

II. EXPERIMENT

The results reported here were obtained using two complementary experimental setups: in Bristol, a home-built time-of-flight (TOF) mass spectrometer was used to record mass resolved $2+1$ REMPI spectra of NH_3 and ND_3, while REMPI-PES studies were performed using a ''magnetic bottle'' spectrometer in Amsterdam. Both experiments have been described in detail previously[41,42] and so only brief summaries of the two experimental methods are given here.

REMPI spectra were recorded using a pulsed nozzle to inject either NH_3 or ND_3 (5% mix in argon, total pressure of ~ 1 atm) into the source region of the TOF mass spectrometer. The gas pulses were crossed by the focused (f.l.$=300$–500 mm) frequency doubled output of a tuneable Nd:YAG pumped dye laser. Wavelength calibration of the dye laser, in the visible, was performed simultaneously with recording of REMPI spectra by measurement of the optogalvanic spectrum of neon excited in a hollow cathode discharge. Ions formed by the focused laser beam in the source region of the mass spectrometer were subjected to two stages of acceleration prior to entering a field-free drift region and

were detected by a pair of chevron-configuration microchannel plates (MCPs). The output signal from the MCPs was accumulated by a digital oscilloscope and downloaded to a computer via a GPIB interface for subsequent analysis. To obtain mass selected REMPI spectra, the dye laser was scanned and only that part of the total ion signal that fell within a narrow time window centered on the TOF of the mass of interest was collected, averaged, and stored. In the spectra so obtained, weak features were identified in the main scan across the spectral range covered in this study and then rerecorded at slower scan speeds and/or enhanced sensitivity.

REMPI-PE spectra were obtained using a XeCl excimer pumped dye laser system with the laser output focused (f.l.$=25$ mm) into the ionization region of the ''magnetic bottle'' electron spectrometer.[41] An effusive beam of pure NH_3 or ND_3 vapor was crossed by the focused laser beam and photoelectrons resulting from each laser pulse were extracted into the spectrometer. The measured times of arrival of the photoelectrons at a pair of MCPs situated at the end of the 500 mm flight tube were used to determine electron kinetic energies. A transient digitizer, interfaced to a PC, recorded preamplified output signals from the MCPs. Kinetic-energy-resolved photoelectron spectra were obtained by progressively stepping the retarding voltage on a grid in the flight tube and, at each voltage setting, performing a time-to-energy transformation on just the slowest (i.e., highest resolution) part of the TOF spectrum, with a resultant 15 meV (FWHM) resolution at all kinetic energies in the present experiments. To place the photoelectron kinetic energies on an absolute scale, the ammonia sample was doped with xenon and well-documented REMPI transitions terminating on the two spin-orbit states of the Xe^+ ion were then used to calibrate the REMPI-PE spectra. Certain wavelength-resolved REMPI spectra were recorded in Amsterdam by measuring both the total and selected energy portion of the photoelectron yield as a function of excitation wavelength.

Spectral analysis of band contours recorded in the REMPI spectra showed that the ammonia molecules in the jet expansion were cooled to ~ 40 K. [The correct nuclear spin statistics for the original room-temperature (298 K) sample of ammonia molecules were incorporated into the simulations.] This should be taken into account in the following section when we compare the REMPI data with the REMPI-PES data which was recorded at 298 K.

III. RESULTS AND DISCUSSION

Figures 2 and 3 show $2+1$ REMPI spectra of NH_3 and ND_3 recorded over the spectral range 68 700–82 200 and 67 200–82 800 cm^{-1}, respectively. The high experimental sensitivity allows extension of all previously observed (by MPI) vibronic progressions associated with the $\widetilde{B}\ ^1E''$, $\widetilde{C}'\ ^1A_1'$, and $\widetilde{E}'\ ^1A_1'$ Rydberg states to energies approaching the lowest ionization limit. These and the new electronic states identified in this work are considered in turn.
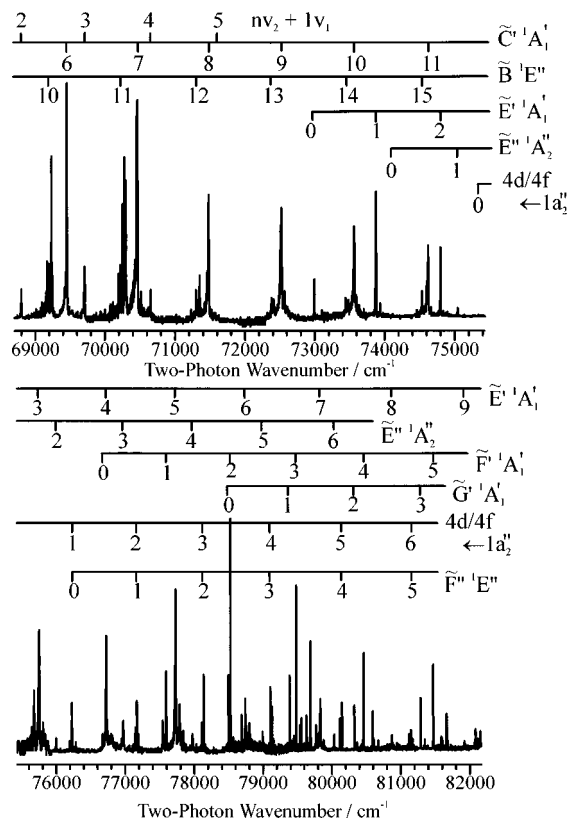
FIG. 2. $2+1$ REMPI spectrum of a jet-cooled sample of NH_3 over the energy range $68\,700$–$82\,160$ cm^{-1} recorded using linearly polarized light and monitoring only those ions with times of flight (TOF) appropriate to m/z 17. This spectrum is a composite, obtaining by splicing together spectra recorded using more than one dye. Although some adjustments were made to avoid serious discontinuities between overlapping spectra, no corrections were made for the variations in the laser output energy. The numbers below the combs festooned in the figure indicate v_2', the upper state out-of-plane bending quantum number of a 2^n vibronic level. The numbers above the $\widetilde{C}'$ state comb indicate the v_2' number of a $1^1 2^n$ vibronic progression.

A. The $\widetilde{B}\,^1E''(3pe''\leftarrow 1a_2'')$ Rydberg state

The recent one (vuv) photon excitation studies of jet-cooled NH_3 and ND_3 molecules by Li and Vidal[21] covered a small portion of the lower energy end of the wavenumber range covered in Figs. 2 and 3. These workers presented rotational analyses for $\widetilde{B}$-$\widetilde{X}\,2_0^n$ bands with $n\leqslant 12$ for both NH_3 and ND_3, thereby extending the database of spectroscopic knowledge which, hitherto, had been restricted to levels with $n\leqslant 8$ (NH_3) and 6 (ND_3).[22,23] The $\widetilde{B}$-$\widetilde{X}\,2_0^n$ bands with $n=10$–12 (NH_3) and $n=11,12$ (ND_3) are evident in the present study also; comparison of simulated band contours with the REMPI data from this study confirms the spectroscopic parameters reported previously for these $\widetilde{B}$ state levels and only the vibronic band origins (ν_0) values are shown in Table I for reference. NH_3 $\widetilde{B}$ state levels with $v_2'>12$ are too heavily predissociated to show resolved rotational structure. The origins for the corresponding $\widetilde{B}$-$\widetilde{X}$ features (evident in Fig. 2 and listed in Table I) were estimated via a band contour analysis described more fully below and in Ref. 43, using extrapolated (not fitted) values for B', C', and ξ, and floating just the band origin ν_0 and the homogeneously broadened linewidth ω_0. In the case of ND_3 it was
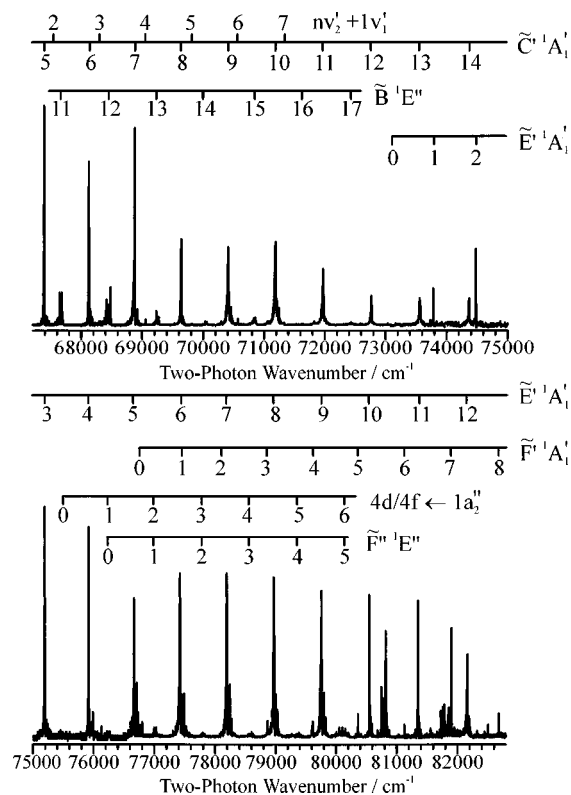

FIG. 3. $2+1$ REMPI spectrum of a jet-cooled sample of ND_3 over the energy range $67\,200$–$82\,800$ cm^{-1} recorded using linearly polarized light and monitoring only those ions with times of flight (TOF) appropriate to m/z 20. Similar to the spectrum in Fig. 2, this is a composite obtained by splicing together spectra recorded using more than one dye. No correct normalization was made for the laser power and the relative intensities of features should be regarded accordingly.

possible to obtain excited state rotational constants from analysis of the $\widetilde{B}$-$\widetilde{X}\,2_0^{13}$ feature [$B'=3.44(8)$ cm^{-1}, $C'=2.82(8)$ cm^{-1}, $\xi=0.78(4)$ with q_ν and the centrifugal distortion constants fixed at 0] which are in accord with the constants for $v_2'<13$, and a homogeneous linewidth for the $v_2'=13$ level [$\omega_0=1.2(2)$ cm^{-1}]. Here too, lack of rota-

TABLE I. Band origins (ν_0) of the predissociated $\widetilde{B}\,^1E''-\widetilde{X}\,^1A_1'\,2_0^n$ transitions in NH_3 and ND_3 determined for $n=10$–12 in the one-photon vuv study of Li and Vidal (Ref. 21) and in this MPI study for $n\geqslant 13$. Band origins for the lower n levels may be found in Refs. 21 and 23. Numbers in parentheses for $n\geqslant 13$ are estimated uncertainties associated with the level of predissociation and interpolation between Ne calibration lines.

| v_2' | ν_0 /cm^{-1} | |
	NH_3	ND_3
10	69 188.20(9)[a]	66 863.33(9)[a]
11	70 250.3(2)[a]	67 652.85(11)[a]
12	71 315.3(2)[a]	68 444.73(10)[a]
13	72 378(2)	69 239(1)
14	73 455(2)	70 015(5)
15	74 513(3)	70 833(3)
16	-	71 623(4)
17	-	72 413(2)

[a]From Ref. 21.

TABLE II. Spectroscopic and linewidth parameters for selected 2^n and $1^1 2^n$ levels of the $\widetilde{C}'$ $^1 A_1'$ states of NH$_3$ and ND$_3$. All excited-state centrifugal distortion constants were clamped to zero in the fitting process. Numbers in parentheses represent the uncertainties returned in the least-squares fitting except in the case of band origins where the quoted errors allow for interpolation between Ne calibration lines.

v_2'		ν_0 /cm^{-1}			
2^n	$1^1 2^{n'}$	NH$_3$		ND$_3$	
$n=4$		67 479(1)		-	
	$n=2$		68 797(1)		67 570(1)
5		68 468(1)		67 392(1)	
	3		69 712(1)		68 312(1)
6		69 457(1)		68 131(1)	
	4		70 654(1)		69 059(1)
7		70 468(1)		68 883(1)	
	5		71 615(5)		69 813(1)
8		71 486(1)		69 645(1)	
	6		72 560(5)		70 568(1)
9		72 529(1)		70 417(1)	
	7		-		71 329(1)
10		73 572(1)		71 194(1)	
11		74 629(1)		71 982(1)	
12		75 679(1)		72 772(1)	
13		-		73 576(1)	

NH$_3$ $1^1 2^n$	B/cm^{-1}	C/cm^{-1}	W	ω_0/cm^{-1}	a	b
$n=2$	9.78(8)	5.37(2)	1.2[a]	2.3(1)	0.1(1)	-1[a]
3	9.82(4)	5.35(3)	1.2[a]	2.2(4)	0.2(1)	-1[a]
4	9.78(5)	5.36(4)	1.2[a]	1.9(2)	0.7(2)	-1[a]

ND$_3$ 2^n	B/cm^{-1}	C/cm^{-1}	W	ω_0/cm^{-1}	a	b
$n=5$	4.70(2)	2.70(3)	1.1(2)	0.9(2)	0[a]	0[a]
6	4.53(3)	2.76(4)	1.3(2)	1.0(2)	0[a]	0[a]
7	4.38(2)	2.73(3)	1.2[a]	1.2(2)	0[a]	0[a]
8	4.34(19)	2.79(34)	1.2[a]	1.3(2)	0[a]	0[a]

[a]Not floated in least-squares fit.

tional resolution only allowed estimation of ν_0 for $\widetilde{B}$-$\widetilde{X}$ 2_0^n transitions with $n \geq 14$. The ν_0 values so obtained are listed in Table I.

B. The $npa_2'' \leftarrow 1a_2''$ Rydberg series ($n=3$ and 4): The $\widetilde{C}'$ $^1 A_1'$ and $\widetilde{E}'$ $^1 A_1'$ states

Table II lists spectroscopic parameters for the 2^n and $1^1 2^n$ levels of the $\widetilde{C}'$ $^1 A_1'$ states of NH$_3$ and ND$_3$ obtained by least-squares fitting to individual rovibronic transitions (in the case of the better resolved bands) or the overall band contour. Only band origins could be obtained with any certainty in the latter cases. The ν_0 values derived for the $1_0^1 2_0^n$ vibrational progressions accord well with those derived [for the $v_2' \leq 3$ (NH$_3$) and 5 (ND$_3$) levels] in the REMPI-PES study of Miller *et al.*[36] All of these features are dominated by $^Q Q$ (i.e., $\Delta J = 0$, $\Delta K = 0$) transitions associated with the $T_0^0(\mathbf{A})$ zero rank component of the two-photon transition tensor. However, as found recently for the corresponding $\widetilde{E}'$ $-\widetilde{X}$ transitions,[37] there is also a smaller contribution from the $T_0^2(\mathbf{A})$ second rank component, revealed by the presence of weaker O, P, R, and S branch transitions. This is illustrated in Fig. 4, which shows expanded views of the $2+1$ REMPI spectra of the NH$_3(\widetilde{C}' \leftarrow \widetilde{X})$ $1_0^1 2_0^3$ transition [Fig. 4(a)] and the ND$_3(\widetilde{C}' \leftarrow \widetilde{X})$ 2_0^5 band [Fig. 4(b)]. The accompanying simulations were derived as follows: Approximate

excited-state constants (ν_0, B', and C') were first obtained by floating them in a least-squares fit to the measured frequencies of the better resolved features in the experimental spectrum while holding the ground-state constants fixed at the values determined by Urban *et al.* for NH$_3$ (Ref. 44) and ND$_3$ (Ref. 45). The upper state constants were then refined
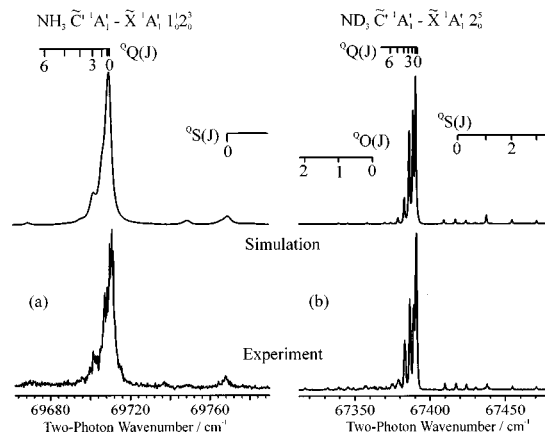

FIG. 4. Jet-cooled $2+1$ REMPI spectrum of (a) the $1_0^1 2_0^3$ band of the NH$_3$ ($\widetilde{C}' \leftarrow \widetilde{X}$) transition and (b) the 2_0^5 band of the ND$_3$ ($\widetilde{C}' \leftarrow \widetilde{X}$) transition, together with the corresponding best-fit simulations (upper curves) of these two-photon excitation spectra obtained using the parameters listed in Table II.

TABLE III. Spectroscopic and linewidth parameters for the ν_2' levels of the $\widetilde{E}'$ $^1A_1'$ state of NH_3 and ND_3. All excited-state centrifugal distortion constants were clamped to zero in the fitting process. Numbers in parentheses represent the uncertainties returned in the least-squares fitting except in the case of band origins where the quoted errors allow for interpolation between Ne calibration lines.

v_2'	ν_0/cm^{-1}	B/cm^{-1}	C/cm^{-1}	W	ω_0/cm^{-1}	a	b
			NH_3 $\widetilde{E}'$ $^1A_1'$ state				
0	72 995(1)	10.54(7)[a]	5.09(1)[a]	1.9(3)[a]	1.2(2)[a]	0.28(10)	−1.02(3)
1	73 878(1)	9.89(9)[a]	5.15(2)[a]	1.9(2)	2.2(6)	0.16(14)	−1[c]
2	74 800(1)	9.87(5)	5.27(4)	1.8(1)	2.7(2)	0.20(22)	−1[c]
3	75 751(1)	9.81(5)	5.12(3)	1.7(1)	3.8(2)	0.4(1)	−1[c]
4	76 732(1)	[b]					
5	77 733(1)	[b]					
6	78 744(3)[e]	[b]					
7	79 831(4)[e]	[b]					
8	80 875(4)[e]	[b]					
			ND_3 $\widetilde{E}'$ $^1A_1'$ state				
0	73 145(1)	5.343(6)[a]	2.620(6)[a]	1.5[c]	1.4[c]	[d]	[d]
1	73 783(1)	5.233(7)[a]	2.647(6)[a]	1.3(8)	1.6(4)	[d]	[d]
2	74 479(1)	5.108(3)[a]	2.670(1)[a]	1.4(2)	1.5(2)	[d]	[d]
3	75 194(1)	5.023(7)[a]	2.684(3)[a]	1.8(3)	2.4(3)	[d]	[d]
4	75 925(1)	4.870(7)[a]	2.770(8)[a]	2.2(1)	2.1(4)	[d]	[d]
5	76 672(1)	4.756(2)[a]	2.718(2)[a]	1.6(1)	2.5(1)	[d]	[d]
6	77 430(1)	4.626(5)[a]	2.743(5)[a]	1.6(1)	3.3(3)	[d]	[d]
7	78 200(1)	4.516(6)[a]	2.741(4)[a]	1.2(1)	2.0(3)	[d]	[d]
8	78 979(1)	4.26(5)	2.74(5)	1.5(2)	2.2(3)	[d]	[d]
9	79 762(1)	4.12(6)	2.80(2)	1.6(2)	2.0(4)	[d]	[d]
10	80 552(1)	3.97(5)	2.81(5)	1.2[c]	1.5(4)	[d]	[d]
11	81 360(1)	3.91(3)	2.80(4)	1.2[c]	1.4(5)	[d]	[d]
12	82 166(1)	3.7(1)	2.76(6)	1.2[c]	1.9(6)	0.3(2)	−1[c]

[a]Taken from Ref. 35.
[b]Insufficient resolved rotational structure to obtain accurate constants.
[c]Not floated in least-squares fit.
[d]Fixed at zero in least-squares fit.
[e]Heavily predissociated, $\omega_0 \sim 10$ cm^{-1}.

using a more elaborate least-squares fit to the experimental band contour rather than the line positions using the procedure described in Ref. 43. This was necessary as even apparently well-resolved ''lines'' generally consist of several transitions with the same values of J or K. Fitting to the band contour allowed due weight to be given to these unresolved transitions, and was essential for other bands which showed little resolved rotational structure. Up to seven additional parameters were floated in the band contour fits: W, ω_0, a, b, temperature, and a simple vertical scaling and offset with no physical significance. W is the ratio of the $T_0^2(\mathbf{A})$:$T_0^0(\mathbf{A})$ transition amplitudes. ω_0 is the linewidth (assumed to be Lorentzian) of transitions involving the rotationless excited state level with $J'=K'=0$. The contribution from the laser bandwidth (estimated as a 0.4 cm^{-1} FWHM Gaussian function at the two-photon energy) has been deconvoluted from all the ω_0 values quoted in this paper. We have not checked carefully for any possible laser power dependence of these widths, but no indication of any such dependence was found during the simulations of any of the data. The parameters a and b allow for the possibility that the excited-state lifetime is rotational level dependent, as is the case for the higher 2^n vibronic levels of the $\widetilde{C}'$ state of NH_3.[24,31,32] Each rotational line is given a further width according to the formula (1):

$$\omega_{J',K'} = \omega_0\{1 + a[J'(J'+1) + bK'^2]\}. \tag{1}$$

None of the fits of individual bands of ND_3 returned statistically significant values for a or b and so these parameters were clamped at zero in the final fits of the $ND_3(\widetilde{C}'-\widetilde{X})$ vibronic bands. In NH_3, however, though the homogeneous predissociation rate is seen to be largely insensitive to increasing v_2', the overall predissociation rate of the higher J,K levels increase via an increasing heterogeneous contribution. The comparability of the rotational constants for any 2^n level[32,37] and the corresponding 1^12^n level highlights the harmonic nature of the ν_1' (symmetric stretching) mode. Allen *et al.*[29] also noted the insensitivity of the $\widetilde{C}'$ state rotational constants to excitation of ν_1' and that the isotopic ratio $\nu_1'(NH_3):\nu_1'(ND_3) \approx 1.38$ is very close to the $\sqrt{2}$ value expected for a harmonic vibration.[25]

Spectroscopic constants for the $\widetilde{E}'$ $^1A_1'$ state, the next ($n=4$) member in the same $npa_2'' \leftarrow 1a_2''$ Rydberg series, are presented in Table III. The present work yields refined band origins and linewidth parameters, but no improvement in the values of B' and C' for NH_3 levels with $v_2' \leqslant 3$ or ND_3 levels with $v_2' \leqslant 7$, respectively, which are taken from Ref. 37. For any given v_2' level, the rotational constants show striking similarities with those of the corresponding $\widetilde{C}'$ $^1A_1'$ state level, as might be expected for Rydberg states belonging to a series converging to the same ion core. Finally we note that, for a given v_2' level in the $\widetilde{C}'$ and $\widetilde{E}'$ states of any

TABLE IV. Spectroscopic and linewidth parameters for the v'_2 levels of the $\widetilde{F}'$ $^1A'_1$ states of NH_3 and ND_3 and the $\widetilde{G}'$ $^1A'_1$ state of NH_3. All excited-state centrifugal distortion constants were clamped to zero in the fitting process. Numbers in parentheses represent the uncertainties returned in the least-squares fitting except in the case of band origins where the quoted errors allow for interpolation between Ne calibration lines.

v'_2	ν_0/cm^{-1}	B/cm^{-1}	C/cm^{-1}	W	ω_0/cm^{-1}	a	b
			NH_3 $\widetilde{F}'$ $^1A'_1$ state				
0	76 674(1)	10.6[a]	5.15[a]	1.2[b]	1.2[a]	0.3(1)	-1[b]
1	77 593(1)	10.3[a]	5.35[a]	1.2[b]	1.2[a]	1.5(2)	-1[b]
2	78 523(1)	9.85[a]	5.7[a]	1.2[b]	0.3(1)	1.3(2)	-1[b]
3	79 479(1)	9.8[a]	5.65[a]	1.2[b]	0.3(1)	1.8(2)	-1[b]
4	80 464(1)	9.75[a]	5.7[a]	1.2[b]	0.4(1)	1.7(2)	-1[b]
5	81 470(1)	9.7[a]	5.65[a]	1.2[b]	0.4(2)	2.0(2)	-1[b]
			ND_3 $\widetilde{F}'$ $^1A'_1$ state				
0	76 770(5)[c]						
1	77 440(5)[c]						
2	78 130(5)[c]						
3	78 870(2)	5.05[a]	2.75[a]	1.2[b]	1.6(3)	0[b]	0[b]
4	79 621(1)	4.9[a]	2.8[a]	1.2[b]	2.2(4)	0[b]	0[b]
5	80 368(1)	4.8[a]	2.8[a]	1.2[b]	1.7(2)	0[b]	0[b]
6	81 133(1)	4.7[a]	2.85[a]	1.2[b]	0.7(2)	0[b]	0[b]
7	81 902(1)	4.6[a]	2.85[a]	1.2[b]	0.4(1)	0.89(5)	-1[b]
			NH_3 $\widetilde{G}'$ $^1A'_1$ state				
0	78 494(1)	10.6[a]	5.1[a]	1.2[b]	0.5(2)	0.2(1)	-1[b]
1	79 387(1)	9.9[a]	5.2[a]	1.2[b]	2.2(2)	0.3(1)	-1[b]
2	80 329(1)	9.7[a]	5.3[a]	1.2[b]	1.4(3)	0.3(3)	-1[b]
3	81 291(1)	9.6[a]	5.3[a]	1.2[b]	1.2(4)	2.0(5)	-1[b]

[a]Determined using the procedure described in the text, with an estimated error of <0.05 cm^{-1}.
[b]Not floated in least-squares fit.
[c]Estimated from REMPI-PES data and isotope shift (see text).

given isotopomer, the values of ω_0, a, and b are also very similar, suggesting that the same homogeneous and heterogeneous predissociation mechanisms are active and that their relative rates (cf. NH_3 and ND_3) are likely to be similar.

The main aim of this study was to clarify the REMPI spectrum of ammonia at energies above the $\widetilde{E}'$ state origin (at $\sim$73 000 cm^{-1}) and up to the first ionization energy. Five clear progressions have been identified amongst the myriad of new features seen in this work; these are now discussed in turn.

C. The $\widetilde{F}'$ $^1A'_1(5pa''_2 \leftarrow 1a''_2)$ Rydberg state

Two of the five progressions will be shown to belong to the same $npa''_2 \leftarrow 1a''_2$ Rydberg series as the $\widetilde{C}'$ and $\widetilde{E}'$ states and are indicated in Figs. 2 and 3; spectroscopic parameters for both NH_3 and ND_3 are listed in Table IV. The appearance of each feature is similar to those observed in the $\widetilde{C}' - \widetilde{X}$ and $\widetilde{E}' - \widetilde{X}$ progressions, characteristic of a parallel two-photon transition from the ground electronic state, while their spacings are indicative of progressions in ν'_2. Unambiguous proof of the quantum number labeling shown in Table IV comes from analysis of the REMPI-PE spectra recorded following excitation at energies resonant with these features. As has been demonstrated many times previously,[46–50] the analysis of such spectra can provide considerable insight into the vibrational and electronic characteristics of the intermediate state providing resonant enhancement which often cannot be obtained in any other way.

Figures 5(a) and 5(b) show representative REMPI-PE spectra associated with features belonging to the $\widetilde{F}' - \widetilde{X}$ progressions in NH_3 and ND_3. Consider the spectrum shown in Fig. 5(a), recorded at a wavelength of 260.77 nm ($2\widetilde{\nu} = 76 674$ cm^{-1}), the deduced origin of this progression in
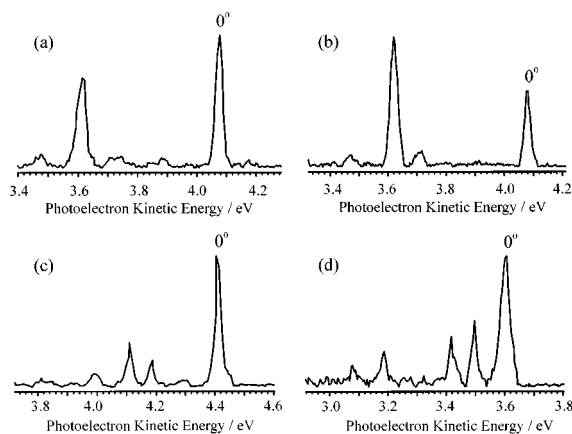

FIG. 5. REMPI-PE spectra of a room-temperature sample obtained following excitation of (a) NH_3 at 260.77 nm ($2\widetilde{\nu} = 76 674$ cm^{-1}), (b) ND_3 at 260.422 nm ($2\widetilde{\nu} = 76 776$ cm^{-1}), (c) NH_3 at 254.72 nm ($2\widetilde{\nu} = 78 495$ cm^{-1}), and (d) NH_3 at 269.75 nm ($2\widetilde{\nu} = 74 119$ cm^{-1}). On the basis of the measured photoelectron kinetic energies we deduce that these two photon resonances involve the 0^0_0 bands of, respectively, transitions to the NH_3 ($\widetilde{F}'$ $^1A'_1$), ND_3 ($\widetilde{F}'$ $^1A'_1$), NH_3 ($\widetilde{G}'$ $^1A'_1$), and NH_3 ($\widetilde{F}''$ $^1A''_2$) Rydberg states. The other peaks that are not labeled in the spectra are discussed in the text.

NH_3. The kinetic energy (KE) of the larger, faster peak (4.08 eV) is entirely consistent with three-photon ionization yielding parent ions in the zero-point level and this, together with REMPI-PES data for the other member of this progression, and the expected propensity for $\Delta v = 0$ transitions upon ionization from a Rydberg member belonging to a series converging to the same ion core, leads us to conclude that REMPI proceeds via an electronic (Rydberg) origin level at $\sim 76\,674$ cm^{-1}. The other peak (at KE=3.62 eV) indicates formation of some ions carrying ~ 0.46 eV of internal energy. This corresponds to four quanta of ν_2^+, the parent ion bending vibration, and appears as an inevitable consequence of the overlapping $\widetilde{E}' - \widetilde{X}\, 2_0^4$ band at the two-photon energy. In fact, the $\widetilde{C}' - \widetilde{X}\, 2_0^{13}$ band also contributes to the room-temperature two-photon excitation spectrum at this energy and, indeed, the corresponding peak can be seen in the REMPI-PE spectrum at KE=2.45 eV.

Use of the modified form of the Rydberg formula[51]

$$\nu = \text{IE} - R/(n - \delta)^2, \tag{2}$$

where IE is the ionization energy for forming the parent ion in $v=0$, gives a value of $(n-\delta)=4.48$. Taking the principal quantum number $n=5$ implies a quantum defect of $\delta = 0.52$ for this state, which would be fully consistent with an assignment involving electron promotion to a p Rydberg orbital. Given the parallel nature of the transition, we conclude that the observed progression is associated with the next ($n=5$) member in the npa_2'' (i.e., np_z)$\leftarrow 1a_2''$ Rydberg series of ammonia. Further support for this assignment comes from the close similarity between its quantum defect and that for the $\widetilde{C}'\, ^1A_1'$ ($\delta = 0.56$) and $\widetilde{E}'\, ^1A_1'$ ($\delta = 0.54$) states. Following the ''historical'' convention for labeling the electronic states of ammonia,[7] we label this state the $\widetilde{F}'\, ^1A_1'$ Rydberg state.

The rotational constants for any given level of the $\widetilde{C}'\, ^1A_1'$ and $\widetilde{E}'\, ^1A_1'$ states are very similar. It might therefore be expected that the same will hold true for the $\widetilde{F}'\, ^1A_1'$ state levels. Such a presumption proved particularly useful when starting to simulate the experimental data, since all of the observed bands are devoid of resolved rotational structure. Thus the B' and C' rotational constants were initially fixed at the average values derived for the corresponding level of the $\widetilde{C}'$ and $\widetilde{E}'$ states, and then manually adjusted to improve the fit of the calculated line positions of the more intense transitions to any partially resolvable structure on the REMPI feature. These structural constants were then fixed while a least-squares band contour fit was performed to determine most of the remaining parameters. The values so derived for the 2^n levels of the $\widetilde{F}'$ state of NH_3 are shown in Table IV. The lack of resolvable structure meant that it was not possible to float all of the parameters and W and b were clamped at 1.2 and -1, respectively. Such values are sensible and consistent with those found for the $\widetilde{C}'$ and $\widetilde{E}'$ states (see above). Figures 6(a) and 6(b) show expanded views of the $2+1$ REMPI spectra of the NH_3 ($\widetilde{F}' \leftarrow \widetilde{X})2_0^2$ and 2_0^3 bands along with two accompanying best-fit simulations of each band, showing the typical signal level and quality of fit for this progression. The two simulations are calculated assuming zero (middle panel) and nonzero (top panel)
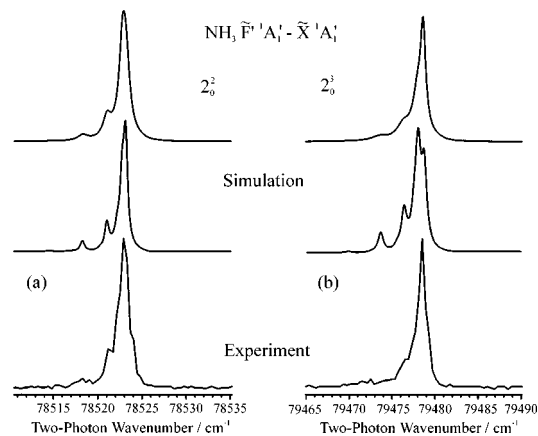

FIG. 6. Jet-cooled $2+1$ REMPI spectrum of (a) the 2_0^2 band and (b) the 2_0^3 band of the NH_3 ($\widetilde{F}' \leftarrow \widetilde{X}$) transition, together with the corresponding best-fit simulations of these two-photon excitation spectra obtained using the parameters listed in Table IV, but either fixing the a and b linewidth parameters to zero (middle) or to the nonzero values given in the Table (top).

values of the linewidth parameters a and b, using the same rotational temperature and floating the linewidth parameter ω_0 in both fits. By fixing a and b to zero, a bigger linewidth is needed in the best-fit [Fig. 2(a): $\omega_0 = 0.5(1)$ cm^{-1} cf. 0.3(1) cm^{-1} for $a,b \neq 0$; Fig. 2(b): $\omega_0 = 0.6(1)$ cm^{-1} cf. 0.3(1) cm^{-1} for $a,b \neq 0$] but this is not sufficient to remove the resolved rotational fine structure and maintain a good fit to the experimental data. It is clear from these simulations that the linewidths show a J', K' dependence. Again, the bands are dominated by $T_0^0(\mathbf{A})$ Q branch transitions, but also show weaker O, P, R, and S branch features associated with the $T_0^2(\mathbf{A})$ component of the two-photon transition tensor.

One interesting point regarding the $\widetilde{F}'$ state of NH_3 is the v_2' dependence of the linewidth parameters (see Table IV). The homogeneous linewidth ω_0 falls, to ~ 0.3 cm^{-1}, for levels with $v_2' \geq 2$. This is in stark contrast to the order of magnitude larger ω_0 values found for the $\widetilde{C}'$ and $\widetilde{E}'$ states of NH_3, which increase with increasing v_2'. Such observations suggest that the homogeneous predissociation mechanism evident in the $\widetilde{C}'$ and $\widetilde{E}'$ states is less efficient for the $\widetilde{F}'$ state, especially when $v_2' \geq 2$. The larger ω_0 values deduced for the 0^0 and 2^1 levels may well reflect their accidental close resonance to dark dissociative states whose coupling to these $\widetilde{F}'$ levels may be mediated by the nearby $\widetilde{E}'$ 2^4 and 2^5 levels, a near degeneracy that tunes out of resonance with increasing v_2'.

As discussed above, the nonzero values of a and b deduced for the NH_3 $\widetilde{F}'$ state levels (Table IV) provide clear indication of a heterogeneous contribution to the overall predissociation. A good fit to the data required use of $b=-1$, as for the $\widetilde{C}'$ and $\widetilde{E}'$ states, consistent with all three of these $^1A_1'$ symmetry states predissociating via an x,y (in-plane) rotationally induced (Coriolis) coupling. This rotation transforms as e'' in D_{3h}, implying that the A_1'/A_2'' vibronic levels of the $\widetilde{F}'$ state of NH_3 predissociate via coupling to dissociative states of E''/E' vibronic symmetry. The magnitudes of the parameter a used in modeling the ''unperturbed'' ($v_2' \geq 2$) levels are bigger than the values obtained for the
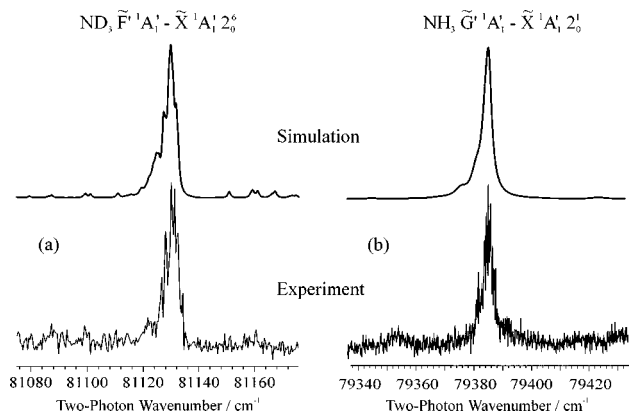
FIG. 7. Jet-cooled $2+1$ REMPI spectrum of (a) the 2_0^6 band of the ND_3 ($\widetilde{F}' \leftarrow \widetilde{X}$) transition and (b) the 2_0^1 band of the NH_3 ($\widetilde{G}' \leftarrow \widetilde{X}$) transition, together with the corresponding best-fit simulations (upper curves) of these two-photon excitation spectra obtained using the parameters listed in Table IV.

corresponding $\widetilde{E}'$ levels in NH_3. This largely reflects the reduced homogeneous predissociation width (ω_0) for these $\widetilde{F}'$ levels and the fact that we choose to parametrize the heterogeneous contribution to the predissociation width in terms of the product $\omega_0 a$ [Eq. (1)].

The REMPI-PE spectrum of ND_3 shown in Fig. 5(b) was recorded at a wavelength of 260.422 nm ($2\widetilde{\nu} = 76\,775.5$ cm^{-1}). The strong peak at 4.08 eV is indicative of resonance enhancement by an electronic origin transition, thus confirming the quantum number labeling of the observed ND_3 ν_2' progression shown in Table IV. The other major peak in this spectrum is associated with REMPI via the $\widetilde{E}'$ 2^5 level, transitions to which overlap the $\widetilde{F}' - \widetilde{X}$ 0_0^0 band in the room-temperature $2+1$ REMPI spectrum of ND_3. The weak feature at KE$=3.71$ eV is associated with $\widetilde{E}' - \widetilde{X}$ 2_1^5 hot band in the room-temperature REMPI-PE spectrum. The overlap of the weak $\widetilde{F}' - \widetilde{X}$ origin band and the stronger $\widetilde{E}' - \widetilde{X}$ 2_0^5 band prevents precise determination of the former band origin, even in the jet-cooled spectrum. Similar arguments apply to the $\widetilde{F}'$ 2^1 and 2^2 levels, their two-photon absorptions being similarly obscured by the corresponding $\widetilde{E}' - \widetilde{X}$ 2_0^6 and 2_0^7 rotational contours, but the next few members of the $\widetilde{F}' - \widetilde{X}$ out-of-plane bending progression are clearly discernible (Table IV). Given the parallel nature of these bands and their very similar energies to those assigned above in terms of the $\widetilde{F}'$ $^1A_1'$ state of NH_3, we ascribe this progression to the corresponding $\widetilde{F}'$ $^1A_1'$ ($5pa_2'' \leftarrow 1a_2''$) Rydberg state in ND_3. Such an assignment implies an isotope shift $[\nu_0(NH_3) - \nu_0(ND_3)] = -102$ cm^{-1}, very similar to that observed for the electronic origins of the $\widetilde{C}'$ and $\widetilde{E}'$ states (-126 and -130 cm^{-1}, respectively).

The rotational constants shown in Table IV for the $\widetilde{F}' - \widetilde{X}$ 2_0^n progression of ND_3 were obtained in the same way as for NH_3. Figure 7(a) shows an expanded view of the $2+1$ REMPI spectrum of the ND_3($\widetilde{F}' \leftarrow \widetilde{X}$) 2_0^6 band and its accompanying simulation. The a parameters were found to be negligible for the ND_3 $\widetilde{F}' - \widetilde{X}$ bands involving $\nu_2' \leq 6$ and were clamped at zero in the final fit. However, we note that
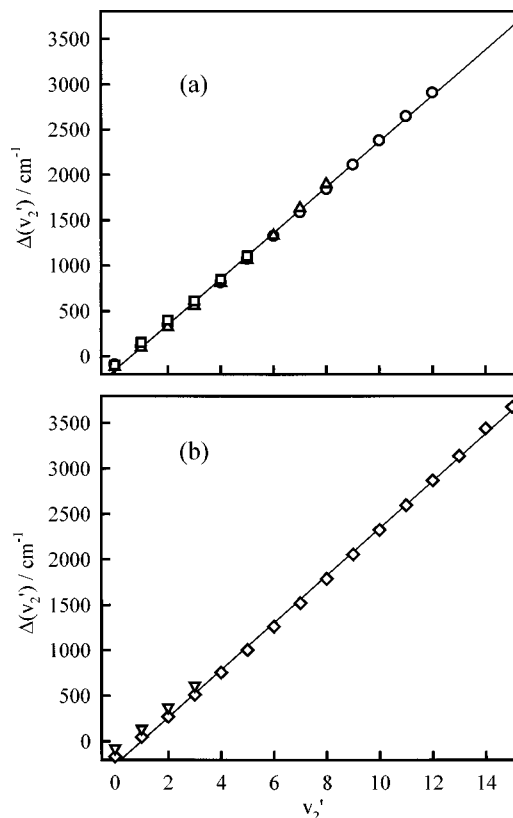

FIG. 8. Isotope shift $\Delta(\nu_2') = \nu_0^{\nu_2'}(NH_3) - \nu_0^{\nu_2'}(ND_3)$ versus the out-of-plane bending quantum number ν_2', for (a) the $npa_1' \leftarrow 1a_2''$ ($n=3-5$) Rydberg states: $\widetilde{C}'$ $^1A_1'$ ($\bigcirc$) (Refs. 7 and 25), $\widetilde{E}'$ $^1A_1'$ ($\triangle$), and $\widetilde{F}'$ $^1A_1'$ ($\square$) and (b) the $\widetilde{B}$ $^1E''$ ($3pe' \leftarrow 1a_2''$) ($\diamondsuit$) (Ref. 21) and $\widetilde{D}$ $^1E'$ ($3de'' \leftarrow 1a_2''$) ($\triangledown$) (Ref. 33) Rydberg states. The best-fit lines through the data points are also shown in the graphs and are calculated using the more extensive data sets of the $\widetilde{C}'$ and $\widetilde{B}$ states.

the best-fit ω_0 value falls with increasing ν_2', indicating a progressive decline in the homogeneous (vibronic) predissociation of this state, to the extent that the best-fit simulation of the $\widetilde{F}' - \widetilde{X}$ 2_0^7 band requires use of a nonzero a value, together with $b = -1$. This might indicate an accidental close coincidence with a very short-lived background state of E' vibronic symmetry, but is more probably simply a reflection of the fact that the effects of any heterogeneous (Coriolis induced) predissociation will be more apparent when the homogeneous decay rate is slow.

The very similar ν_2' dependence of the isotope shift, $\Delta(\nu_0)$, in the case of the $\widetilde{C}'$ and $\widetilde{E}'$ states of ammonia has been noted previously.[37] Figure 8(a) demonstrates that the $\widetilde{F}'$ state term values show a similar dependence upon isotopic substitution, as expected for (unperturbed) Rydberg states converging to the same ion core, thereby providing further confirmation of the correctness of the proposed vibronic numbering of the $\widetilde{F}' - \widetilde{X}$ progressions in both NH_3 and ND_3.

D. The $\widetilde{G}'$ $^1A_1'$ ($6pa_2'' \leftarrow 1a_2''$) Rydberg state

The REMPI-PE spectrum shown in Fig. 5(c) was obtained following MPI of NH_3 at a wavelength of 254.72 nm ($2\widetilde{\nu} = 78\,495$ cm^{-1}). The strong peak at a kinetic energy of

4.41 eV is consistent with three-photon ionization to the $v^+ = 0$ level of the ion, suggesting that the 254.72 nm resonance is associated with two-photon excitation to a vibrationless level. The REMPI band contour points to this being a parallel transition, while additional PES data involving other members in the v_2' progression confirms the vibrational quantum number labeling shown in Table IV. The weaker features evident in the photoelectron spectrum [Fig. 5(c)] are all explicable in terms of $2+1$ REMPI via near resonant levels of the $\widetilde{C}'$, $\widetilde{D}'''$ $^1E''$, $\widetilde{E}'$, and $\widetilde{F}'$ states, whose room-temperature band contours contribute to the two-photon absorption at this wavelength. Using the modified Rydberg equation gives $(n - \delta) = 5.47$, and a quantum defect of $\delta = 0.53$ (assuming $n = 6$). This δ value is very close to that obtained for the $\widetilde{C}'$, $\widetilde{E}'$, and $\widetilde{F}'$ states of ammonia and we conclude that this progression is associated with a $6pa_2'' \leftarrow 1a_2''$ electronic transition. We label the resulting state the $\widetilde{G}'$ $^1A_1'$ Rydberg state of NH_3.

Band contour simulation (as above) yielded the rotational constants and parameters for this progression as listed in Table IV. Given the poor signal-to-noise ratio associated with these features, the B' and C' constants were not floated in the least-squares fit but set manually, at (roughly) the mean of the values for the corresponding v_2' level of the $\widetilde{C}'$ and $\widetilde{E}'$ states, so as to give a reasonable fit to the observed peak positions. Figure 7(b) shows an expanded view of the $2+1$ REMPI spectrum of the $NH_3(\widetilde{G}' \leftarrow \widetilde{X})$ 2_0^1 band and its accompanying simulation. The deduced predissociation behavior largely parallels that found for the corresponding levels of the $\widetilde{E}'$ and $\widetilde{F}'$ states, though the simulation suggests a marked increase in the heterogeneous predissociation efficiency for the $\widetilde{G}'$ $v_2' = 3$ level. Again, we propose accidental resonance with a short-lived state of E' vibronic symmetry to account for this observation: clearly the chances of accidental resonance increase (simply because of the increased overall state density) as the ionization energy is approached.

Given the characteristic isotope shift dependence shown in Fig. 8(a), we can estimate term values for the analogous $\widetilde{G}' - \widetilde{X}$ 2_0^n progression in ND_3. The predicted values fall very close to other structured bands in the REMPI spectrum (discussed below), but no features unambiguously attributable to a parallel transition have been identified.

E. The $\widetilde{E}''$ $^1A_2''(5sa_1' \leftarrow 1a_2'')$ Rydberg state

The REMPI-PE spectrum of NH_3 shown in Fig. 5(d) was recorded at an excitation wavelength of 269.75 nm ($2\widetilde{\nu} = 74\ 119\ cm^{-1}$). The strong peak at 3.59 eV is consistent with three-photon ionization to the $v^+ = 0$ level of the parent ion and confirms the presence of an electronic origin resonant at the two-photon energy. Again weaker features evident in the photoelectron spectrum can all be assigned in terms of vertical ($\Delta v = 0$) ionization following transitions to near resonant levels of the $\widetilde{C}'$, $\widetilde{D}'''$, and $\widetilde{E}'$ states whose room-temperature band contours contribute to the two-photon absorption at this wavelength. Table V summarizes the observed progression (in v_2') of parallel band features built on this weak origin in the $2+1$ REMPI spectrum (Fig.

2). REMPI-PE spectra recorded for each of these features confirm the authenticity and vibrational quantum number labeling of this progression. Use of the modified Rydberg equation gives a value of $(n - \delta) = 3.59$ for this electronic origin. We consider two possible assignments for this state. If we assume $n = 5$ the origin exhibits a quantum defect of $\delta = 1.41$, which could be consistent with assignment in terms of the $5sa_1' \leftarrow 1a_2''$ electron promotion, resulting in a state of $^1A_2''$ electronic symmetry. The $4da_1' \leftarrow 1a_2''$ excitation will also yield a state of $^1A_2''$ symmetry, but the implied quantum defect ($\delta = 0.41$) would indicate an unusually large degree of core penetration for a d Rydberg orbital which, traditionally, exhibits a quantum defect $\delta \sim 0$. The former assignment, which we favor, associates this progression with the so-called $\widetilde{E}''$ $^1A_2''$ Rydberg state of NH_3. Colson and co-workers[7] attributed a poorly resolved progression in the room-temperature vuv absorption spectrum of ammonia to

TABLE V. Band origins (ν_0) for the predissociated $\widetilde{E}''$ $^1A_2'' - \widetilde{X}$ $^1A_1'$ 2_0^n transitions of NH_3 and ND_3. The ν_0 values and v_2' quantum number labels given in Ref. 7 for this Rydberg state are also shown. Numbers in parentheses represent the uncertainties for interpolation between Ne calibration lines and the level of predissociation.

v_2'		ν_0/cm^{-1}		
			NH_3	
	Ref. 7		Ref. 7	ND_3
0		74 118(2)		74 258(2)
1	0	75 045(2)	74 974	75 021(3)
2	1	75 997(2)	75 861	-
3	2	76 975(3)	76 781	-
4	3	77 975(3)	77 748	-
5	4	78 992(4)	78 740	-
6	-	79 997(5)	-	-

TABLE VI. Band origins (ν_0) and assignments for two overlapping v_2' progressions ($4d/4f \leftarrow 1a_2''$ and $\widetilde{F}''$ $^1E'' \leftarrow 1a_2''$) of "structured" features seen in both the NH_3 and ND_3 $2+1$ REMPI spectra. Also shown are the ν_0 values and v_2' quantum number labels given in Ref. 7 for the $\widetilde{E}$ state of ammonia. Numbers in parentheses represent the uncertainties determined by the width of the feature in the jet-cooled (40 K) $2+1$ REMPI spectrum.

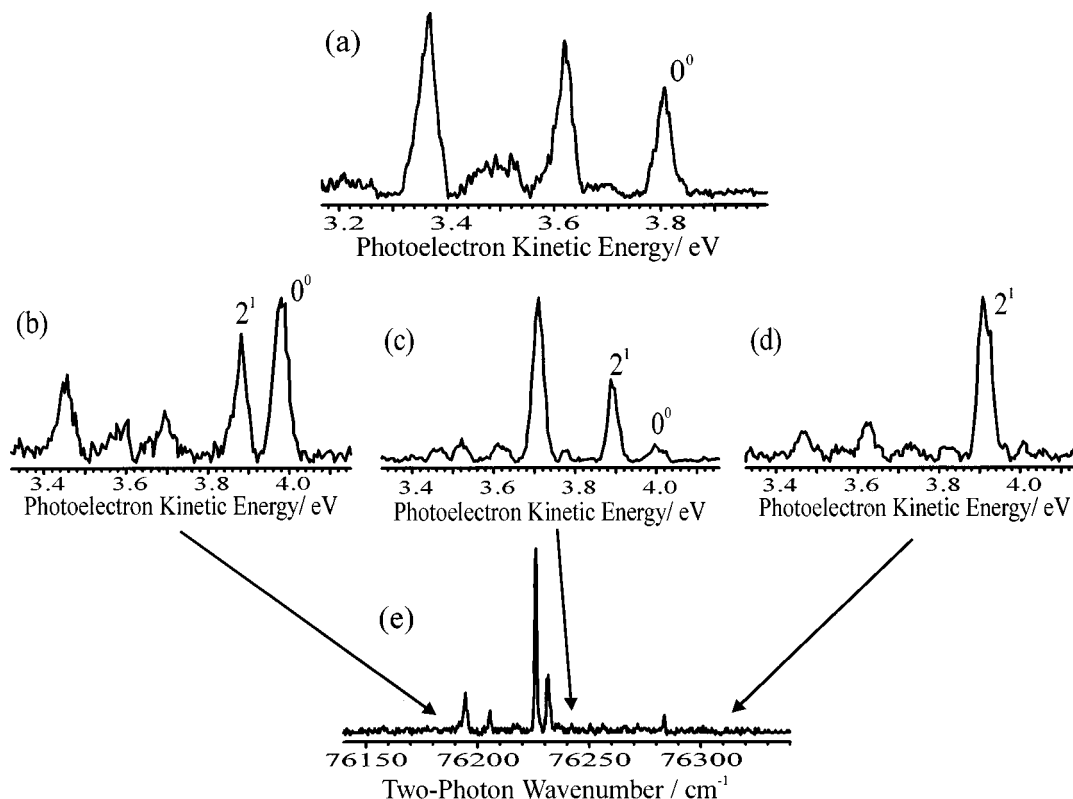| $4d/4f \leftarrow 1a_2''$ v_2'	$\widetilde{F}''$ $^1E''$ v_2'	ν_0/cm^{-1}	v_2' $\widetilde{E}$ (Ref. 7)	ν_0/cm^{-1} (Ref. 7)
		NH_3		
0		75 335(10)	0	75 205
1	0	76 200(50)	1	76 121
2	1	77 160(50)	2	77 079
3	2	78 130(50)	3	78 042
4	3	79 120(50)	4	79 029
5	4	80 130(50)	5	80 042
6	5	81 140(50)	-	-
		ND_3		
0		75 480(50)	0	75 458
1	0	76 240(50)	1	76 217
2	1	77 010(50)	2	76 984
3	2	77 790(50)	3	77 779
4	3	78 580(50)	4	78 580
5	4	79 370(50)	-	-
6	5	80 180(50)	-	-

FIG. 9. REMPI-PE spectra of NH_3 obtained following excitation at (a) 265.12 nm ($2\widetilde{\nu}=75\,334$ cm^{-1}). The strong peak at high kinetic energies (3.81 eV) is consistent with ionization to the $\nu^+=0$ level of the ion. (b) 262.465 nm ($2\widetilde{\nu}=76\,178$ cm^{-1}), (c) 262.251 nm ($2\widetilde{\nu}=76\,240$ cm^{-1}), and (d) 261.956 nm ($2\widetilde{\nu}=76\,326$ cm^{-1}). For reference, part of the jet-cooled NH_3 $2+1$ REMPI spectrum within the $2\widetilde{\nu}$ energy range of the REMPI-PE spectra in (b)–(d) is shown in (e) (The three $2\widetilde{\nu}$ energies are indicated in (e) by the arrows. Note that the REMPI-PES data were taken with a room-temperature sample). The two strong peaks at high kinetic energies in (b) are concordant with ionization from a 0^0 and 2^1 level of the neutral molecule. The other peaks that are not labeled in the spectra are discussed in the text.

this $\widetilde{E}''$ state. Allowing for the breadth of the absorption features, the two data sets are in satisfactory agreement if the earlier v_2' vibrational numbering is increased by one.

The observation of a member of the $nsa_1'\leftarrow 1a_2''$ Rydberg series in the MPI spectrum of NH_3 might seem surprising considering that the lower energy $(n=4)$ $\widetilde{D}'$ $^1A_2''$ state is not observed in this or previous REMPI studies. This nonobservation is presumably indicative of a high predissociation rate for the $\widetilde{D}'$ state, consistent with the breadth and diffuseness of the $\widetilde{D}'-\widetilde{X}$ 2_0^n features in the one-photon absorption spectrum.[7] This can be rationalized in terms of efficient homogeneous coupling to the very short-lived $\widetilde{A}$ $^1A_2''(3sa_1'\leftarrow 1a_2'')$ state, a coupling which can be expected to decline with an increase in principal quantum number on account of the increasing energy mismatch and the scaling of the coupling matrix element with $n^{-3/2}$. At the same time, however, the two-photon oscillator strength is expected to decrease with increasing principal quantum number. This, allied with the increasing spectral congestion, may account for our nonobservation of series members with $n>5$.

The signal-to-noise ratios associated with the observed $\widetilde{E}''-\widetilde{X}$ features are quite low and, as a result, we only estimate ν_0 values by least-squares band contour fitting with all other excited-state parameters clamped at values appropriate for the corresponding 2^n levels associated with the $npa_2''\leftarrow 1a_2''$ Rydberg series members (Tables II–IV).

Approximate term values (ν_0) for the $\widetilde{E}''-\widetilde{X}$ 2_0^n progression in ND_3 can be calculated assuming the previously recognized isotope shift dependence (Fig. 8). Unfortunately, apart from the 0_0^0 and 2_0^1 features they are all obscured by the rotational contours of the more intense $\widetilde{E}'-\widetilde{X}$ 2_0^n $(n\geqslant 4)$ bands. The experimentally derived ν_0 values for transitions involving the $\widetilde{E}''$ 0^0 and 2^1 levels are shown in Table V.

F. $4d/4f\leftarrow 1a_2''$ and $5pe'\leftarrow 1a_2''$ Rydberg states

The two other new progressions identified in this REMPI study are less clear cut than the three progressions of parallel bands discussed above. Many of the remaining unassigned features in the NH_3 $2+1$ REMPI spectrum fit to a plausible progression in ν_2', starting with a "single" feature at 75 334 cm^{-1} and continuing up to the ionization energy as a series of increasingly structured bands (see Table VI). Investigation of these features using REMPI-PE spectroscopy turns out to be mandatory to reveal a rather congested picture.

Figure 9(a) shows the REMPI-PE spectrum of NH_3 recorded at an excitation wavelength of 265.12 nm ($2\widetilde{\nu}=75\,334$ cm^{-1}). The appearance of a strong peak at 3.81 eV, indicative of parent ion formation in its zero-point level, identifies an electronic origin resonant at the two-photon energy. The kinetic energies of the two other peaks in this

spectrum indicate formation of ions carrying, respectively, 0.19 and 0.44 eV of internal energy, neither of which are readily explicable in the light of our discussion thus far. The former corresponds to no integer multiple of ν_2^+ but is consistent with ν_4^+.[24,38] Energetic considerations therefore suggest some (accidental) involvement from the $\widetilde{E}'' 4^1$ level in the $2+1$ REMPI process at this wavelength. We note for future reference that this level will have $^1E''(^1A_2'' \otimes e')$ vibronic symmetry. Given the Franck–Condon propensities associated with vertical excitations in ammonia the most attractive interpretation of an internal energy of 0.44 eV must be $4\nu_2^+$. None of the parallel progressions discussed above show a 2_0^4 band at this energy, but the previously documented $\widetilde{D}''' \ ^1E'' - \widetilde{X}(4pe' \leftarrow 1a_2'')$ transition does,[7] and we propose that it is two-photon resonance enhancement associated with this excited level that is responsible for the slowest photoelectron peak evident in Fig. 9(a). Use of the modified Rydberg equation yields a value $(n-\delta)=4.01$ and a quantum defect $\delta = -0.01$ if we assume $n=4$, characteristic of an electronic excitation to a d- or f-Rydberg orbital. Attempts to model the 75 334 cm^{-1} feature in terms of a $^1A_1'$ $-\widetilde{X} \ ^1A_1'$ or $^1A_2'' - \widetilde{X} \ ^1A_1'$ two-photon transition (such as might arise as a result of the respective $4fa_2'' \leftarrow 1a_2''$ or $4fa_1' \leftarrow 1a_2''$ excitation), or as $^1E'' - \widetilde{X} \ ^1A_1'$ (e.g., $4de'$ $\leftarrow 1a_2''$ or $4fe' \leftarrow 1a_2''$) or $^1E' - \widetilde{X} \ ^1A_1'$ (e.g., $4de'' \leftarrow 1a_2''$ or $4fe'' \leftarrow 1a_2''$) two-photon transitions, all proved inconclusive but, given the deduced symmetry of the other vibronic levels contributing to the two-photon resonance enhancement, it is tempting to suspect that the deduced electronic origin may have $^1E''$ electronic symmetry and that vibronic mixing (and accidental near-coincidence in energy) accounts for the unexpected showing of the ν_4^+ feature in the REMPI-PE spectrum [Fig. 9(a)].

Figures 9(b)–9(d) show REMPI-PE spectra of NH$_3$ recorded at excitation wavelengths of 262.465 nm ($2\widetilde{\nu}$ $=76\ 178$ cm^{-1}), 262.251 nm ($2\widetilde{\nu}=76\ 240$ cm^{-1}), and 261.956 nm ($2\widetilde{\nu}=76\ 326$ cm^{-1}), resonant with what appears to be the next member ($v_2'=1$) in the bending progression built on the 75 334 cm^{-1} origin (see Table VI). For reference, an expanded view of the relevant part of the $2+1$ REMPI spectrum of jet-cooled ammonia molecules is shown in Fig. 9(e). However, it must be remembered that the corresponding REMPI-PE spectrum were taken with a much warmer parent sample under which conditions the structure in Fig. 9(e) is more dispersed. Clearly, the form of the REMPI-PE spectra vary sensitively according to the precise excitation wavelength, pointing to contributory resonance enhancements from more than one intermediate level. All three spectra show a peak at a kinetic energy ~ 3.9 eV, consistent with REMPI terminating on the $v_2^+=1$ level of the ion and with our presumption that the 2^1 level built on the 75 334 cm^{-1} origin must contribute to the two-photon resonance enhancement at these energies. The peak at KE~ 3.71 eV evident in Fig. 9(c) is consistent with $2+1$ REMPI via the $\widetilde{E}'' \ 2^1 4^1$ level, again paralleling behavior deduced for REMPI via the 75 334 cm^{-1} feature. More surprisingly, however, the strongest peak in Fig. 9(b) (at a KE of 3.98 eV) indicates ion formation in the $v^+=0$ level and thus
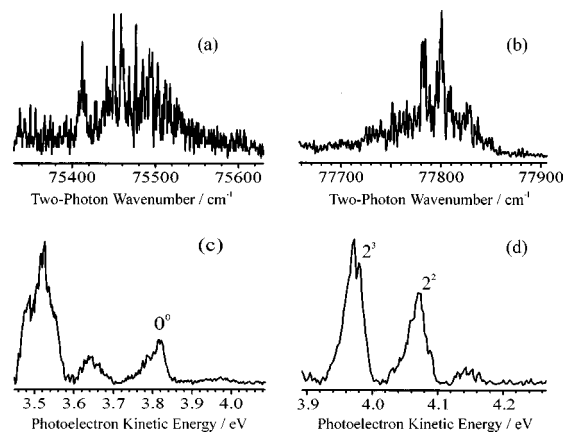

FIG. 10. (a) and (b) Two parts of the jet-cooled ND$_3$ $2+1$ REMPI spectrum within the $2\widetilde{\nu}$ resonant energy range of the REMPI-PE spectra [(c) and (d)] obtained following excitation, respectively, at (c) 265.0 nm ($2\widetilde{\nu}$ $=75\ 450$ cm^{-1}) and (d) 257.0 nm ($2\widetilde{\nu}=77\ 790$ cm^{-1}). The peaks that are labeled in (c) and (d) are consistent with ionization from the level indicated in the neutral ND$_3$ molecule. The other peaks that are not labeled in the spectra are discussed in the text.

the presence of another origin level at $\sim 76\ 200$ cm^{-1}. REMPI-PE spectra obtained when exciting via higher members of this presumed progression show a generally similar pattern. In each case we observe photoelectron peaks indicative of $2+1$ REMPI via the respective 2^n levels built on the origins at $\sim 75\ 334$ and $\sim 76\ 200$ cm^{-1}, and via the corresponding near resonant $\widetilde{E}'' \ 2^n 4^1$ vibronic level. Thus (apart from vibronic contributions) the photoelectron data suggests that the ''structured'' progression evident in the REMPI spectrum of NH$_3$ involves contributions from at least two electronic states with origins at $\sim 75\ 334$ and $\sim 76\ 200$ cm^{-1}. Using the modified Rydberg equation (2) we obtain a quantum defect value $\delta \sim 0.66$ (assuming $n=5$) which suggests that we are dealing with an excitation populating a p Rydberg orbital. All the evidence points to the $\widetilde{F}'' \ ^1E''(5pe' \leftarrow 1a_2'')$ state being responsible for the $\sim 76\ 200$ cm^{-1} origin; the relative ordering of the $\widetilde{F}'' \ ^1E''(5pe' \leftarrow 1a_2'')$ and $\widetilde{F}' \ ^1A_1'(5pa_2'' \leftarrow 1a_2'')$ states mimics that of the thoroughly documented $\widetilde{B}$ and $\widetilde{C}'$ states arising from the corresponding $3p \leftarrow 1a_2''$ electron promotion.

The features in the $2+1$ MPI spectrum of ND$_3$ (Table VI) that appear to correspond to this progression in NH$_3$ all have a similar appearance, i.e., a number of sharp features on top of a broad background [see Figs. 10(a) and 10(b)]. The REMPI-PES data associated with this ''progression'' of features shows many similarities with that seen for NH$_3$. Figure 10(c) shows the REMPI-PE spectrum recorded at an excitation wavelength of 265.0 nm (75 450 cm^{-1}). The highest energy feature (at 3.82 eV) is associated with formation of parent ions in their $v^+=0$ state, implying the presence of an electronic origin providing resonance enhancement at the two-photon energy. The energy difference between this two-photon resonance and the 75 334 cm^{-1} origin in NH$_3$ is fully consistent with the isotope shifts identified for other Rydberg origins in NH$_3$ and ND$_3$ (recall Fig. 8) and we similarly assign this electronic origin in ND$_3$ in terms of a $4d/4f$ $\leftarrow 1a_2''$ electron promotion. The most intense peak in Fig.

J. Chem. Phys., Vol. 108, No. 16, 22 April 1998

Langford *et al.* 6679

TABLE VII. Approximate band origins (ν_0), quantum defects (δ), and provisional assignments of five new Rydberg states of NH_3 obtained from the analysis of the v_2^+ value of the dominant ion product in REMPI-PES spectra recorded at a resonant energy near the ionization potential.

v_2^+	ν_0 /cm^{-1}	δ	Assignment
a	77 860(10)	~0.05	$(5d/5f \leftarrow 1a_2'')0_0^0$
2	79 694(5)		2_0^2
3	80 608(5)		2_0^3
4	81 562(5)		2_0^4
0	79 295(5)	~0.81	$\widetilde{H}''\ ^1E''(7pe' \leftarrow 1a_2'')0_0^0$
0	79 560(5)	~0.50	$\widetilde{H}'\ ^1A_1'(7pa_2'' \leftarrow 1a_2'')0_0^0$
2	81 395(5)		2_0^2
a	80 020(10)	~0.82	$\widetilde{I}''\ ^1E''(8pe' \leftarrow 1a_2'')0_0^0$
1	80 935(5)		2_0^1
0	80 225(5)	~0.47	$\widetilde{I}'\ ^1A_1'(8pa_2'' \leftarrow 1a_2'')0_0^0$
1	81 125(5)		2_0^1

[a]Not observed in the REMPI-PE spectrum but extrapolated from the band origin of the other features in the v_2' progressions.

TABLE VIII. Electronic origins and quantum defects, δ, of the new Rydberg states of ammonia observed in this study.

State	ν_0 /cm^{-1}		δ[a]
	NH_3	ND_3	
$\widetilde{E}''\ ^1A_2''(5sa_1' \leftarrow 1a_2'')$	74 118(2)	74 258(2)	1.41
$4d/4f \leftarrow 1a_2''$	75 340(10)	75 480(50)	0.01
$\widetilde{F}''\ ^1E''(5pe' \leftarrow 1a_2'')$	76 220(50)	76 240(50)	~0.70
$\widetilde{F}'\ ^1A_1'(5pa_2'' \leftarrow 1a_2'')$	76 674(1)	76 770(5)	0.56
$\widetilde{G}'\ ^1A_1'(6pa_2'' \leftarrow 1a_2'')$	78 494(1)	-	0.53
$(5d/5f \leftarrow 1a_2'')$	77 860(10)	-	0.05
$\widetilde{H}''\ ^1E''(7pe' \leftarrow 1a_2'')$	79 295(5)	-	0.81
$\widetilde{H}'\ ^1A_1'(7pa_2'' \leftarrow 1a_2'')$	79 560(5)	-	0.50
$\widetilde{I}''\ ^1E''(8pe' \leftarrow 1a_2'')$	80 020(10)	-	0.82
$\widetilde{I}'\ ^1A_1'(8pa_2'' \leftarrow 1a_2'')$	80 225(5)	-	0.47

[a]From the NH_3 data.

10(c), appearing at a kinetic energy of ~3.52 eV, indicates a propensity for forming ND_3^+ ions in their $v_2^+ = 3$ level. This can be understood in terms of $\Delta v = 0$ ionization following transition to the near resonant $\widetilde{E}'\ 2^3$ level, the room-temperature band contour which contributes to the two-photon absorption at this wavelength. Somewhat surprisingly, REMPI-PES measurements at the slightly longer wavelength of 265.12 nm (75 416 cm^{-1}) show this weak feature [evident in REMPI spectrum shown in Fig. 10(a)] to be associated with the $\widetilde{F}' - \widetilde{X}\ 2_2^0$ hot band transition. Analogy with NH_3 suggests that we should find evidence for the corresponding $\widetilde{F}''\ ^1E''(5pe' \leftarrow 1a_2'')$ transition at slightly higher energy. Its origin band would be expected to fall within the broad resonance centered at ~76 250 cm^{-1}, but appears to be too weak for certain identification. However, the REMPI-PE spectra show clear evidence of the $\widetilde{F}'' - \widetilde{X}\ 2_0^n$ progression at higher energies. Figure 10(d), obtained following excitation at 257.0 nm (77 790 cm^{-1}), shows one example: the peaks appearing at 4.07 and 3.97 eV are indicative of parent ion formation in the $v_2^+ = 2$ and 3 states, and are most readily explained in terms of $2+1$ REMPI via, respectively, the $\widetilde{F}''\ 2^2$ and $4d/4f\ 2^3$ levels.

G. Other features

Figures 2 and 3 serve to emphasize that the $2+1$ REMPI spectrum of ammonia, particularly NH_3, becomes increasingly congested at energies approaching the first ionization energy. Much of this structure is sufficiently sharp to encourage expectations that it should be interpretable by, for example, two-color double resonance spectroscopy experiments involving well-characterized levels of the $\widetilde{B}$ or $\widetilde{C}'$ states. Here we merely list (Table VII) vibronic assignments of some of the more intense features in the REMPI spectrum of NH_3 as deduced from kinetic energy analysis of the accompanying photoelectrons. Quantum defect considerations lead to the tentative interpretations proposed in Table VII.

Yet again, we note the dominance of the $np \leftarrow 1a_2''$ transitions in the $2+1$ REMPI spectrum of this molecule.

IV. CONCLUSION

This paper presents detailed measurements of the $2+1$ REMPI spectrum of ammonia (both NH_3 and ND_3) at higher energies than hitherto, up to the first ionization energy. Complementary analyses of the wavelength resolved REMPI spectrum and the accompanying REMPI-PE spectra has led to the identification of ten new Rydberg origins of the NH_3 molecule (four in the case of ND_3) which are summarized in Table VIII and, in most cases, the accompanying out-of-plane bending vibrational progressions. Upper state rotational constants and qualitative predissociation rates for several of the observed vibronic levels have also been calculated using a least-squares band contour analysis.

Finally, we note from Fig. 8 that the average isotope shift of the origin level for the observed Rydberg states of ammonia is $\langle \nu_0(NH_3) - \nu_0(ND_3) \rangle = 120 \pm 40$ cm^{-1}. Assuming that the quantum defects of the Rydberg states of ND_3 will be very similar to the corresponding states in NH_3, the adiabatic ionization energy of ND_3 can be estimated as $82\ 280 \pm 40$ cm^{-1}.

[1] A. B. F. Duncan, Phys. Rev. **47**, 822 (1935); **50**, 700 (1936).
[2] A. E. Douglas and J. M. Hollas, Can. J. Phys. **39**, 479 (1961).
[3] A. E. Douglas, Discuss. Faraday Soc. **35**, 158 (1963).
[4] A. D. Walsh and P. A. Warsop, Trans. Faraday Soc. **57**, 345 (1961).
[5] M. N. R. Ashfold, C. L. Bennett, and R. J. Stickland, Comments At. Mol. Phys. **19**, 181 (1987) and references therein.
[6] G. C. Nieman and S. D. Colson, J. Chem. Phys. **68**, 5656 (1978); **71**, 571 (1979).

[7] J. H. Glownia, S. J. Riley, S. D. Colson, and G. C. Nieman, J. Chem. Phys. **72**, 5998 (1980); **73**, 4296 (1980).

[8] M. N. R. Ashfold and J. D. Prince, Contemp. Phys. **29**, 125 (1988) and references therein.

[9] A. D. Walsh, J. Chem. Soc. **1953**, 2296.

[10] R. S. Mulliken, J. Chem. Phys. **3**, 506 (1935).

[11] L. D. Ziegler, J. Chem. Phys. **82**, 664 (1985).

[12] M. N. R. Ashfold, C. L. Bennett, and R. N. Dixon, Chem. Phys. **93**, 293 (1985); Faraday Discuss. Chem. Soc. **82**, 163 (1986).

[13] J. Xie, G. Sha, X. Zhang, and C. Zhang, Chem. Phys. Lett. **124**, 99 (1986).

[14] S. A. Henck, M. A. Mason, W. B. Yan, K. K. Lehmann, and S. L. Coy, J. Chem. Phys. **102**, 4783 (1995); **102**, 4772 (1995).

[15] M. I. McCarthy, P. Rosmus, H.-J. Werner, P. Botschwina, and V. Vaida, J. Chem. Phys. **86**, 6693 (1987).

[16] J. Biesner, L. Schnieder, J. Schmeer, G. Ahlers, X. Xie, K. H. Welge, M. N. R. Ashfold, and R. N. Dixon, J. Chem. Phys. **88**, 3607 (1988); **91**, 2901 (1989).

[17] M. N. R. Ashfold, R. N. Dixon, S. J. Irving, H.-M. Koeppe, W. Meier, J. R. Nightingale, L. Schnieder, and K. H. Welge, Philos. Trans. R. Soc. London, Ser. A **332**, 375 (1990).

[18] D. H. Mordaunt, M. N. R. Ashfold, and R. N. Dixon, J. Chem. Phys. **104**, 6460 (1996); **104**, 6472 (1996).

[19] R. N. Dixon, Mol. Phys. **88**, 949 (1996).

[20] V. Vaida, W. Hess, and J. L. Roebber, J. Phys. Chem. **88**, 3397 (1984).

[21] X. Li and C. R. Vidal, J. Chem. Phys. **101**, 5523 (1994); **102**, 9167 (1995).

[22] M. N. R. Ashfold, R. N. Dixon, R. J. Stickland, and C. M. Western, Chem. Phys. Lett. **138**, 201 (1987).

[23] M. N. R. Ashfold, R. N. Dixon, N. Little, R. J. Stickland, and C. M. Western, J. Chem. Phys. **89**, 1754 (1988).

[24] M. R. Dobber, W. J. Buma, and C. A. de Lange, J. Phys. Chem. **99**, 1671 (1995).

[25] G. Herzberg, Molecular Spectra and Molecular Structure, Vol 2. Infrared and Raman Spectra of Polyatomic Molecules (Van Nostrand Reinhold, New York, 1945).

[26] J. M. Allen, M. N. R. Ashfold, R. J. Stickland, and C. M. Western, Mol. Phys. **74**, 49 (1991).

[27] T. Seeleman, P. Andresen, and E. W. Rothe, Chem. Phys. Lett. **146**, 89 (1988).

[28] J. M. Allen, M. N. R. Ashfold, R. J. Stickland, and C. M. Western, J. Chem. Soc., Faraday Trans. **86**, 2921 (1990).

[29] J. M. Allen, M. N. R. Ashfold, C. L. Bennett, and C. M. Western, Chem. Phys. Lett. **149**, 1 (1988).

[30] X. Li, X. Xie, L. Li, X. Wang, and C. Zhang, J. Chem. Phys. **97**, 128 (1992).

[31] M. N. R. Ashfold, R. N. Dixon, and R. J. Stickland, Chem. Phys. **88**, 463 (1984).

[32] M. N. R. Ashfold, R. N. Dixon, K. N. Rosser, R. J. Stickland, and C. M. Western, Chem. Phys. **101**, 467 (1986).

[33] J. H. Glownia, S. J. Riley, S. D. Colson, J. C. Miller, and R. N. Compton, J. Chem. Phys. **77**, 68 (1982).

[34] Y. Achiba, K. Sato, K. Shobotake, and K. Kimura, J. Chem. Phys. **78**, 5474 (1983).

[35] W. E. Conaway, R. J. S. Morrison, and R. N. Zare, Chem. Phys. Lett. **113**, 429 (1985).

[36] P. J. Miller, S. D. Colson, and W. A. Chupka, Chem. Phys. Lett. **145**, 183 (1988).

[37] M. N. R. Ashfold, C. M. Western, J. W. Hudgens, and R. D. Johnson III, Chem. Phys. Lett. **260**, 27 (1996).

[38] W. Habenicht, G. Reiser, and K. Muller-Dethlefs, J. Chem. Phys. **95**, 4809 (1991); **98**, 8462 (1993).

[39] M. Suto and L. C. Lee, J. Chem. Phys. **78**, 4515 (1983).

[40] C. J. Apps, M. J. Bramwell, J. L. Cooper, J. C. Whitehead, and F. Winterbottom, Mol. Phys. **83**, 1265 (1994).

[41] B. G. Koenders, D. W. Wieringa, K. E. Drabe, and C. A. de Lange, Chem. Phys. **118**, 13 (1987).

[42] R. A. Morgan, A. J. Orr-Ewing, D. Ascenzi, M. N. R. Ashfold, W. J. Buma, C. R. Scheper, and C. A. de Lange, J. Chem. Phys. **105**, 2141 (1996).

[43] T. J. Slotterback, S. G. Clement, K. C. Janda, and C. M. Western, J. Chem. Phys. **101**, 7221 (1994).

[44] S. Urban, R. D'Cunha, K. N. Rao, and D. Papousek, Can. J. Phys. **62**, 1775 (1984).

[45] S. Urban, D. Papousek, M. Bester, K. Yamada, G. Winnewisser, and A. Guarnieri, J. Mol. Spectrosc. **106**, 29 (1984).

[46] M. N. R. Ashfold and J. D. Howe, Annu. Rev. Phys. Chem. **45**, 57 (1994) and references therein.

[47] R. A. Morgan, A. J. Orr-Ewing, M. N. R. Ashfold, W. J. Buma, N. P. L. Wales, and C. A. de Lange, J. Chem. Soc., Faraday Trans. **91**, 3339 (1995).

[48] R. A. Morgan, M. A. Baldwin, A. J. Orr-Ewing, M. N. R. Ashfold, W. J. Buma, J. B. Milan, and C. A. de Lange, J. Chem. Phys. **104**, 6117 (1996).

[49] R. A. Morgan, A. J. Orr-Ewing, D. Ascenzi, M. N. R. Ashfold, W. J. Buma, C. R. Scheper, and C. A. de Lange, J. Chem. Phys. **105**, 2141 (1996).

[50] R. A. Morgan, M. A. Baldwin, D. Ascenzi, A. J. Orr-Ewing, M. N. R. Ashfold, W. J. Buma, J. B. Milan, C. P. Scheper, and C. A. de Lange, Int. J. Mass Spectrom. Ion Processes **159**, 1 (1996).

[51] M. B. Robin, Higher Excited States of Polyatomic Molecules (Academic, New York, 1974), Vols. 1 and 2.